



Published in final edited form as:

*ACS Appl Mater Interfaces*. 2016 January 27; 8(3): 2423–2434. doi:10.1021/acsami.5b11811.

## Sundew-Inspired Adhesive Hydrogels Combined with Adipose-Derived Stem Cells for Wound Healing

Leming Sun<sup>†,‡</sup>, Yujian Huang<sup>†,‡</sup>, Zehua Bian<sup>†,§</sup>, Jennifer Petrosino<sup>||</sup>, Zhen Fan<sup>†,‡</sup>,  
Yongzhong Wang<sup>†,‡</sup>, Ki Ho Park<sup>‡,§</sup>, Tao Yue<sup>†,‡</sup>, Michael Schmidt<sup>†</sup>, Scott Galster<sup>#</sup>, Jianjie  
Ma<sup>‡,§</sup>, Hua Zhu<sup>\*,‡,§,⊥</sup>, and Mingjun Zhang<sup>\*,†,‡,⊥</sup>

<sup>†</sup>Department of Biomedical Engineering, College of Engineering, The Ohio State University, Columbus, Ohio 43210, United States

<sup>‡</sup>Dorothy M. Davis Heart & Lung Research Institute, The Ohio State University, Columbus, Ohio 43210, United States

<sup>§</sup>Department of Surgery, The Ohio State University, Columbus, Ohio 43210, United States

<sup>||</sup>Biomedical Sciences Graduate Program, College of Medicine, The Ohio State University, Columbus, Ohio 43210, United States

<sup>⊥</sup>Interdisciplinary Biophysics Graduate Program, The Ohio State University, Columbus, Ohio 43210, United States

<sup>#</sup>711th Human Performance Wing, Air Force Research Laboratory, Wright-Patterson AFB, Ohio 45433-7901, United States

### Abstract

The potential to harness the unique physical, chemical, and biological properties of the sundew (*Drosera*) plant's adhesive hydrogels has long intrigued researchers searching for novel wound-healing applications. However, the ability to collect sufficient quantities of the sundew plant's adhesive hydrogels is problematic and has eclipsed their therapeutic promise. Inspired by these natural hydrogels, we asked if sundew-inspired adhesive hydrogels could overcome the drawbacks associated with natural sundew hydrogels and be used in combination with stem-cell-based therapy to enhance wound-healing therapeutics. Using a bioinspired approach, we synthesized adhesive hydrogels comprised of sodium alginate, gum arabic, and calcium ions to mimic the properties of the natural sundew-derived adhesive hydrogels. We then characterized and showed that these sundew-inspired hydrogels promote wound healing through their superior adhesive strength, nanostructure, and resistance to shearing when compared to other hydrogels in vitro. In vivo, sundew-inspired hydrogels promoted a "suturing" effect to wound sites, which was

\*Corresponding Authors Hua.Zhu@osumc.edu. Tel.: 001-614-292-2130. zhang.4882@osu.edu. Tel.: 001-614-292-1591.

#### Author Contributions:

L.S. and Y.H. contributed equally to this work.

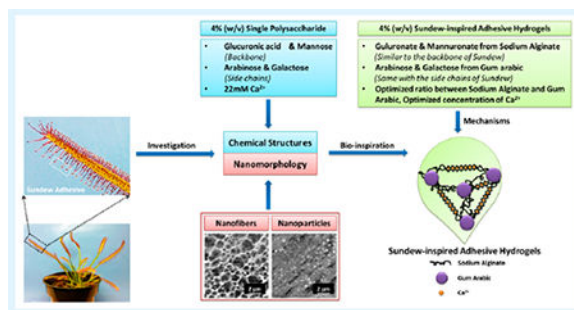
#### Notes:

The authors declare no competing financial interest.

The Supporting Information is available free of charge on the ACS Publications website at DOI: 10.1021/acsami.5b11811.

Adhesive forces measured by AFM and FTIR spectra of the sodium alginate, gum arabic, S1G1, and S1G1Ca10 samples; evaluation of organs (brain, heart, liver, lung, kidney, and spleen) toxicities by H&E staining; analysis of inflammatory factors TNF- $\alpha$ , IL-6, and the tissue injury marker LDH expressed by control, gum arabic, sodium alginate, S1G1, and S1G1Ca10. (PDF)

demonstrated by enhanced wound closure following topical application of the hydrogels. In combination with mouse adipose-derived stem cells (ADSCs) and compared to other therapeutic biomaterials, the sundew-inspired hydrogels demonstrated superior wound-healing capabilities. Collectively, our studies show that sundew-inspired hydrogels contain ideal properties that promote wound healing and suggest that sundew-inspired-ADSCs combination therapy is an efficacious approach for treating wounds without eliciting noticeable toxicity or inflammation.



## Keywords

sundew adhesive; bioinspiration; adhesive hydrogels; ADSCs; wound healing

## INTRODUCTION

Wound healing is a remarkably dynamic and complex process that requires the activation and coordination of cellular pathways regulating inflammation, proliferation, and remodeling to restore tissue homeostasis and integrity following injury.<sup>1</sup> Given the complexity of this physiological process, significant concerns have been raised in regards to pathologies that arise from impaired wound healing such as ischemia, bacterial colonization, senescence, and fibrotic regeneration.<sup>2,3</sup> Many novel wound-healing materials have been created with the development of modern medical science and technology.<sup>4-6</sup> Chitosan, collagen, alginate, peptide, and polyurethane are common biomaterials that are utilized for wound-healing applications.<sup>7-11</sup> However, these common materials have various limitations that result from poor mechanical properties and unsuitable water vapor transmission rates. The most concerning is their poor anti-infective properties that can lead to infection, dehydration, and maceration of wounds.<sup>12,13</sup> To date, biomedical engineering has faced major challenges in developing bioactive, biocompatible, and cost-effective materials capable of stimulating the wound repair process. Therefore, the grand challenge of designing and synthesizing new biocompatible and bioactive wound-healing biomaterials is constantly undergoing investigation.

Adhesive hydrogels secreted from the leaves of sundew (*Drosera*) have long attracted researchers' interests because of their unique physical, chemical, and biological properties. Early studies demonstrated that sundew's unique adhesive architecture consists of an intricate network of nanofibers and nanoparticles.<sup>14</sup> Thus, their organization generates a hydrogel with high water content (96%), viscoelastic adhesion, and biocompatibility.<sup>15,16</sup> Furthermore, sundew adhesive hydrogels can facilitate the differentiation and attachment of

certain fibroblastlike cells,<sup>14,17</sup> making the hydrogel highly suitable for wound-healing applications.

A limitation perturbing the advancement of sundew-derived wound-healing therapeutics is their low yield from the plant. Several *in vitro* studies have been conducted to improve the yield; however, none have been close to supplying the demand.<sup>18,19</sup> Because the structural traits and morphological characteristics of sundew adhesive hydrogels are known,<sup>15-18</sup> there is a large opportunity to synthesize sundew-inspired or -mimetic adhesive hydrogels with wound-healing applications. The schematic in Figure 1 demonstrates the design and fabrication of sundew-inspired adhesive hydrogels. The natural sundew adhesive hydrogel is a 4% (w/v) single acidic polysaccharide with a characteristic backbone containing repeating dimers of glucuronic acid and mannose.<sup>20,21</sup> The polysaccharides are assembled with the assistance of inorganic cations such as calcium ions ( $\text{Ca}^{2+}$ ). Additionally, the monosaccharides arabinose and galactose form the sundew adhesive's side chains.<sup>20</sup> Because of the linear arrangement of nanoparticle-derived nanofibers, the sundew adhesive hydrogel is an excellent accelerator for wound healing.

Inspired by the chemical structure and nanomorphology of the sundew adhesive, sodium alginate, gum arabic, and  $\text{Ca}^{2+}$  were used to synthesize the sundew-inspired adhesive hydrogels. Sodium alginate, a natural anionic polysaccharide, was used for the sundew-inspired hydrogel's backbone. This seaweed-derived biomaterial, which is composed of mannuronate and guluronate, has a structure analogous to that of the backbone of sundew adhesive. In commercial industries, it is a commonly used biomaterial because of its biocompatibility and ease of gelation.<sup>22</sup> Furthermore, acidic residues exist on the backbones of the sundew-inspired and natural sundew hydrogels, promoting the idea that the polysaccharide assembly in both materials is bridged by divalent cations. Of note, because alginate hydrogels have been particularly attractive in wound healing, drug delivery, and tissue engineering,<sup>23</sup> their effects were compared to the sundew-inspired hydrogels throughout the course of our investigations. Additionally, gum arabic was selected to make the side chains of the sundew-inspired hydrogels because of its composition of arabinose and galactose, two monosaccharides also found in the sundew adhesive hydrogel's side chains. Similar to sodium alginate, gum arabic is a polysaccharide that has been extensively used in pharmaceutical, cosmetic, and food industries<sup>24</sup> as a means to cover inflamed surfaces in the intestinal mucosa. Furthermore, it has antibacterial and antioxidant activities that potentiate the wound-healing process.<sup>25,26</sup> In the sundew adhesive hydrogels,  $\text{Ca}^{2+}$  drives the cross-linking reaction that occurs between the polysaccharides and the electrostatic interactions that are essential for the gelation process.  $\text{Ca}^{2+}$  has an established role in the regulation of mammalian skin homeostasis and serves as a key modulator in keratinocyte proliferation and differentiation.<sup>27</sup> Recent *in vitro* studies using keratinocyte and dermal fibroblasts have identified  $\text{Ca}^{2+}$  as a key modulator of epidermal regeneration and dermal reconstruction. This is due to its regulation of cell lipid barrier function, proliferation, and maturation during the wound-healing process.<sup>28-30</sup>

Given the critical role of epidermal stem cells in wound healing and the multifarious differentiation capabilities of pluripotent stem cells, significant efforts have been focused on the development of stem-cell-based therapies with wound-healing applications. Many early

wound-healing cell-based therapies were focused on utilizing embryonic stem cells (ESC); however, there has been a shift to utilizing mesenchymal stem cells (MSC) in recent years. The stromal fraction of adipose contains a population of MSCs known as adipose-derived stem cells (ADSCs). These cells are considered to be superior to ESCs because they can be isolated in large quantities without extensive ethical considerations. Furthermore, they have been shown to increase neovascularization,<sup>31,32</sup> enhance recruitment of other cell types to the site of injury,<sup>33,34</sup> and promote growth and migration among surrounding cells,<sup>35,36</sup> thus promoting the differentiation of keratinocytes and epithelial cells<sup>37,38</sup> involved in the wound-healing process.

In this study, we set out to investigate if sundew-inspired hydrogels alone or in combination with ADSCs could enhance the wound-healing process and overcome the limitations of naturally and commercially available hydrogels. To do this, we first synthesized sundew-inspired hydrogels and then tested their *in vivo* and *in vitro* wound-healing capabilities against alternative biomaterials. Our optimization and biological experiments as well as our efficacy and toxicity studies showed that sundew-inspired hydrogels are a superior biomaterial for wound-healing applications. When combined with ADSCs and compared to alternative biomaterials, the combination therapy proved to be superior for accelerating the early stages of wound repair. It could be that in this combination therapy the ADSCs function as a natural ointment whereas the hydrogel serves as a synthetic bandage. Thus, the additive benefits of their intrinsic pro-wound-healing properties work synergistically to promote an ideal environment for the repair and regeneration of cutaneous wounds.

## EXPERIMENTAL SECTION

### Materials and Animals

Sodium alginate and calcium chloride dehydrate were purchased from Sigma-Aldrich (St. Louis, MO, USA). Gum arabic was purchased from Biosupplies Australia Pty., Ltd. (La Trobe Uni, Bundoora, Australia). Sundew (*Drosera capensis*) was obtained from local nurseries (Columbus, OH, USA). Fetal calf serum (FCS), penicillin, and streptomycin were purchased from Hyclone Laboratories (Logan, UT, USA). The DMEM/F12 cell culture medium was purchased from ATCC (Manassas, VA, USA). Other chemicals were ordered from Sigma-Aldrich (St Louis, MO, USA). All reagents used in this article were analytic reagent (AR)-grade and used as received.

Female C57BL/6J (10 weeks of age; Jackson Laboratory, Bar Harbor, ME, USA) were singly housed with 12 h light and dark cycles and maintained on a standard chow diets. Single housing was implemented to prevent fighting and attack on the wounds. The Institutional Animal Care and Use Committee (IACUC) at The Ohio State University approved all animal use procedures, and all necessary efforts were executed to minimize the animal suffering.

### Adhesive Hydrogels Synthesis

The adhesive hydrogels were formed through the reaction of sodium alginate, gum arabic, and CaCl<sub>2</sub>. First, 4% (w/v) sodium alginate and gum arabic were dissolved in deionized

water for 1 h stirring, respectively. Then, seven different sundew-inspired samples were separately prepared according to the ratios of sodium alginate (S)/gum arabic (G) (S1G1, 1:1; S1G2, 1:2; S1G3, 1:3; S2G1, 2:1; S2G3, 2:3; S3G1, 3:1; and S3G2, 3:2) and maintained at a concentration of 4% (w/v). Three candidate hydrogels (S1G2, S2G1, and S1G1) were selected for further investigation according to their significant differences in chemical and physical properties. Of those three, S1G1 was determined to be the best hydrogel candidate, and differential concentrations of  $\text{Ca}^{2+}$  were introduced to the sample (1, 5, 10, 15, 20, and 25 mM). Three concentrations of  $\text{Ca}^{2+}$ , 5, 10, and 15 mM, were selected for further investigation because of their significant difference in chemical and physical properties. A summary of the chemical concentrations and the code names for the biomaterials (sodium alginate, gum arabic, S1G2, S2G1, S1G1, S1G1Ca5, S1G1Ca10, and S1G1Ca15) are detailed in Table 1.

### Lap Shear Adhesion Test

We first tested the adhesive properties of the top-performing sundew-inspired adhesive hydrogels. To do this, glass slides were soaked for 24 h in a mixture of  $\text{H}_2\text{SO}_4$  and  $\text{H}_2\text{O}_2$  (7:3, v/v), rinsed with deionized water, and oven-dried at 65 °C. The adhesive performances of the hydrogels was analyzed with a lap shear test using the Instron E1000 testing system (Instron, Norwood, MA, USA) with  $\pm 1000$  N dynamic capacity at room temperature. A 50  $\mu\text{L}$  sample of the adhesive hydrogels was added to each glass slide and then overlapped at 1 in.  $\times$  1 in. This was the setup of the lap shear test. After overlapping the slides, the samples were clamped together by two binder clips with a force of  $\sim 25$  N, and repeated measurements ( $n = 5$  per sample) were taken.

### Dynamic Light Scattering

The size distribution of nanoparticles in gum arabic was evaluated by dynamic light scattering (DLS) at 25 °C using a Malvern Zetasizer Nano (Malvern Instruments Ltd., Malvern, Worcestershire, UK). The measurements were performed in triplicate ( $n = 3$ ).

### Morphology Characterization Using Atomic Force Microscopy

Gum arabic, sodium alginate, and the sundew-inspired adhesive hydrogel S1G1Ca10 were scanned for the existence of nanostructures using the MFP-3D atomic force microscopy (AFM) system (Asylum Research, Santa Barbara, CA, USA) with an ACTA-50 Probe from AppNano (Mountain View, CA, USA). The silicon tip has a pyramidal shape with radius of curvature (ROC) below 10 nm. The silicon cantilever has a rectangular shape with alumina reflex coating. The spring constant of the cantilever was between 13 and 77 N/m and the frequency was between 200 and 400 kHz. The images were recorded with Igor Pro software in AC mode at room temperature, thus minimizing potential distortive effects from mechanical interactions between the AFM tip and surface.

### Adhesive Force Measurement Using AFM

Equal volume samples were deposited onto freshly cleaned coverslips by spin-coating at 500 rpm. The adhesive force of the samples were investigated by using force spectroscopy in contact mode with the MFP-3D AFM system and a Veeco MSCT probe with a spring

constant of 2 N/m. The frequency of the cantilever was approximately 17 kHz. A total of 20 curves (consisting of a trace and retrace) were recorded in a grid covering an area of  $4\ \mu\text{m} \times 4\ \mu\text{m}$ . During the experiment, the AFM cantilever applied an average normal force of 10 nN. Force versus sample displacement data were transformed into force–distance curves through shifting of the sample displacement by the indentation depth. All experiments were performed at a room temperature of 25 °C.

### Cell Stiffness Analysis

The MFP-3D AFM system was used to test fibroblast stiffness. To eliminate the confounding effects of neighboring cells on cytoskeletal arrangement and morphology, single-cells measurement were taken using Pyrex-Nitride spherical probes (CP-PNP-PS, NanoAndMore, Watsonville, CA, USA) with a spring constant of 0.08 N/m. The frequency of the cantilever was approximately 10 kHz. The cantilevers were stress-compensated and had a 65 nm chromium/gold backside coating for high laser reflectivity. After various samples' treatments, fibroblast cells were indented over the perinuclear region of individual cells. To stimulate physiological deformations in the best manner, the indentation depth was at least 1  $\mu\text{m}$ . Cell stiffness was determined using force versus indentation curves from each measurement using the Hertzian contact model.<sup>39</sup>

### Rheological Characterization

The rheological analysis was performed using a TA AR2000 rheometer equipped with cone-plate geometry (TA Instruments, New Castle, DE, USA). The cone had an angle of 1° and a diameter of 40 mm. After being equilibrated at 20 °C for 2 min, a shear rate ramp from 0.1 to 100  $\text{s}^{-1}$  at 20 °C was applied for sodium alginate, gum arabic, and the sundew-inspired hydrogels (S2G1, S1G1, S1G2, S1G1Ca5, S1G1Ca10, and S1G1Ca15). All measurements were performed in triplicate ( $n = 3$ ).

### Fourier Transforms Infrared Spectroscopy Analysis

The chemical structures of sodium alginate, gum arabic, S1G1, and S1G1Ca10 were determined using Fourier transform infrared spectroscopy (FTIR). All samples were freeze-dried and mixed with potassium bromide. Triplicate ( $n = 3$ ) transmission spectra were acquired using a Bruker Vertex 70 FT-IR spectrometer (Bruker Corporation, Billerica, MA, USA).

### Cell Culture

The L929 dermal fibroblast and HaCaT keratinocyte cell lines were used as model systems in this study. Stocks of both cell types were maintained under exponential growth in DMEM/F12 culture medium, supplemented with 10% FCS and 1% antibiotics (penicillin/streptomycin). Cells were seeded in 12-well plates (Millipore, Billerica, MA, USA) at a density of  $2 \times 10^5$  cells/well and maintained at 37 °C in a 5%  $\text{CO}_2$  humidified atmosphere. Cells were grown in culture medium supplemented with 10% FCS for 24 h before any cell treatments to attain confluence.

### Scratch Wound Assay

Once confluent, the cell monolayer was scratched in a straight line using a sterile pipet tip to mimic an incision wound. Cells were then washed with PBS to remove debris. Fresh culture medium (10% FBS, 90% DMEM/F12) was added, and the cells were treated with 1 mg/mL sodium alginate, gum arabic, S1G1, sundew, and S1G1Ca10 or nothing (control) and incubated at 37 °C. Wound closure was monitored by collecting digitized images at various time intervals after the scratch was performed and until closure was either complete or no longer progressing. Digital images were captured under an inverted microscope (IX81, Olympus Inc., Shibuyaku, Tokyo, Japan), and the area of the scratch was analyzed using Image-J software. Data presented represents the extent of wound closure (percentage by which the original scratch area has decreased for each given time point). All measurements were performed in triplicate ( $n = 3$ ).

### MTT Assay

The cytotoxicity of sodium alginate, gum arabic, S1G1, and S1G1Ca10 was assessed in L929 and HaCaT cells using colorimetric MTT (3-(4,5-dimethylthiazol-2-yl)-2,5-diphenyltetrazolium bromide, Sigma, St Louis, MO, USA) assays. Cells were first seeded into 96-well plates in 100  $\mu$ L DMEM/F12 culture medium containing 10% FCS at a seeding density of 10 000 cells/well. Cells were then incubated for 2 h at 37 °C to permit cell adhesion and washed repeatedly in serum-free medium. Cells were then maintained in 100  $\mu$ L of culture medium without (control) or with four separate samples of sodium alginate, gum arabic, S1G1, and S1G1Ca10. Following 24 and 48 h incubations, 10  $\mu$ L of MTT solution (5 mg/mL in PBS, pH 7.4) was added to each well and plates were incubated for an additional 4 h. The culture medium was then removed and replaced with 100  $\mu$ L of DMSO. Absorbance was measured at 570 nm by a microplate reader ( $\mu$ Quant, Bio-Tek, Winooski, VT, USA) and cell viabilities were compared to those of the untreated groups. Measurements were done in 5 replicate wells per each condition.

### Isolation and Culture of ADSCs

The adipose tissue was mechanically separated and collected from mice abdomen. After extensive washing with PBS containing 5% penicillin/streptomycin, samples were digested with 0.075% collagenase Type I prepared in PBS with 2% antibiotics (penicillin/streptomycin). The stromal vascular fraction, which contains the ADSCs, was obtained through centrifugation at 2000 rpm for 5 min. ADSCs were enriched on lysine-coated culture plates and incubated at 37 °C, and 5% CO<sub>2</sub> to eliminate red blood cell contamination. Morphological changes in the isolated ADSCs were characterized and monitored using an optical microscope over the course of 3, 5, and 9 days.

### Characterization of ADSCs by Flow Cytometry

ADSCs were detached using 0.2% trypsin-EDTA and counted. Rat serum (3%) was added to aliquots of about  $2 \times 10^5$  cells in centrifuge tubes. The cells were incubated on ice for 30 min, resuspended in PBS, and pelleted by centrifugation for 10 min at 274 g. Cells were then stained with 1  $\mu$ g/mL antibodies (anti-CD73, anti-CD105, anti-CD31, and anti-CD45) at 4 °C for 30 min. The corresponding isotope antibodies were used as negative controls and

goat anti-mouse IgG (H/L); FITC was used as a secondary antibody. The cells were pelleted, washed twice with PBS, and fixed with 1% paraformaldehyde. Fluorescence-activated cell sorting (FACS) was performed (FacsCalibur, BD Biosciences, Franklin Lakes, NJ, USA) and analyzed using Cell Quest software (BD Biosciences). Small and large cells were identified using forward and side-angle scatter plots. To account for autofluorescence, FACS was performed on cells that had not been incubated with fluorochrome-labeled antibodies. Surface antigen expression was determined with a variety of directly labeled antibodies according to the supplier's recommendations.

### Oil Red O Staining

Oil Red O staining was done to evaluate the adipogenic potential of the isolated ADSCs. Culture plates without modification (Bare) and those coated with sundew-derived or -inspired hydrogels were tested to see if they influenced the adipogenic differentiation of ADSCs. Confluent cells (100% confluence, passage 6, day 0) were incubated for 7 days with adipocyte differentiation medium (10  $\mu\text{g}/\text{mL}$  insulin, 1  $\mu\text{M}$  dexamethasone, 0.5 mM 3-isobutyl-1-methylxanthine, and 200  $\mu\text{M}$  indomethacin). To test for the presence of differentiated adipogenic cells, cells were stained with Oil Red O. Cells were fixed, rinsed twice with PBS, and stained with 1 mL of Oil Red O working solution (3:2 dilutions) for 30 min at room temperature. Samples were then thoroughly washed with PBS for several hours to remove nonspecific dye. Images were captured using a Leica DM IL fluorescence microscope (Leica microsystems, Buffalo Grove, IL, USA) using an excitation wavelength of 560 nm and an emission wavelength of 645 nm.

### Excision Wound Model

A full-thickness excision wound model was used to monitor wound closure. All the animals were anesthetized with FORANE (isoflurane, USP), and their dorsal hair was removed using depilatory cream. The surgical area was cleaned with 70% ethanol and then a full-thickness wound (4 mm diameter) was created on the dorsal surface of each mouse using a 4 mm biopsy punch. Wounds were left open and immediately photographed using a digital camera. Animals were divided into five groups ( $n = 6$  mice per group). In the first set of experiments, wounds were topically treated by applying sodium alginate, gum arabic, and sundew-inspired (S1G1 and S1G1Ca10) hydrogels. In later studies, cellulose, mucin, and sundew-derived and -inspired adhesive hydrogels with or without ADSC ( $1 \times 10^6$  cells/50  $\mu\text{L}$ /animal) as well as negative controls (untreated wounds) or positive controls (commercial wound-healing gel) were applied to wounds for the comparison of their wound-healing effects. All the mice were housed individually to prevent additional litter-mate-induced disturbances to the wound area.

For wound closure studies, changes in wound area were measured and photographed on day 4, 7, and 11. Wound closure was calculated using the following formula:

$$\%wound\ closure = (A_0 - A_n) / A_0 \times 100$$

where  $A_0$  is the original wound area and  $A_n$  is the open area of wound at the time of day 4, 7, and 11. At the conclusion of the in vivo studies, all animals were scarified under



anesthesia. Wounds and blood were removed from animals for histological and inflammatory analysis.

### Histology and Inflammation Analysis

Hematoxylin–eosin (H&E) staining was performed on skin, brain, heart, liver, lung, kidney, and spleen samples from each group for toxicity evaluation. Additionally, Masson's trichrome staining was done to investigate the presence of newly formed epithelium, granulation tissue, and collagen deposition. All specimens were fixed in 10% buffered formalin, processed, and embedded in paraffin. Skin specimens (4  $\mu\text{m}$  sections) were sectioned perpendicular to the wound surface according to standard procedures. All sections were analyzed using light microscopy in a blind manner.

Eleven days after wound induction, mouse serum was collected via cardiac puncture for tumor necrosis factor- $\alpha$  (TNF- $\alpha$ ) and interleukin-6 (IL-6) (Invitrogen, Carlsbad, CA, USA) enzyme-linked immunosorbent assays (ELISAs). Commercial enzyme activity kits were used to measure lactate dehydrogenase (LDH) (Clontech Laboratories, Mountain View, CA, USA) using a Flexstation3 plate reader (Molecular Devices, Sunnyvale, CA, USA) according to the manufacturer's directions.

### Statistical Analysis

Data are expressed as mean  $\pm$  SD. In vitro experiments were performed at least in triplicate ( $n = 3$ ). Group comparisons were performed using two-tailed Student's  $t$  test ( $\alpha = 0.05$ ) comparing experimental groups to control, unless otherwise noted.

## RESULTS AND DISCUSSION

### Preparation of Sundew-Inspired Adhesive Hydrogels

Inspired by the chemical structure and nanomorphology of natural sundew adhesive hydrogels, the sundew-inspired adhesive hydrogels were derived from sodium alginate, gum arabic, and  $\text{Ca}^{2+}$ . The sundew-inspired adhesive hydrogels were 4% (w/v), a concentration that is identical to that of natural sundew adhesive hydrogels. The high water content of the sundew-inspired adhesive hydrogels made them excellent candidates for tissue engineering and regenerative medicine.

Sodium alginate was selected to construct the backbone, and gum arabic was selected for the side chains of the sundew-inspired adhesive hydrogels. These biomaterials are analogous to those that make up the backbone and side chains of sundew adhesive hydrogels. Specifically, sodium alginate and the backbone of sundew adhesive hydrogels are acidic polysaccharides made of repeating glucuronic acid and mannose dimers. Additionally, gum arabic comprises arabinose and galactose, two monosaccharides found in the side chains of the sundew adhesive. Sodium alginate and gum arabic also contain intrinsic wound-healing properties that made them excellent biomaterials for the synthesis of sundew-inspired adhesive hydrogels with wound-healing applications. After we established that sodium alginate (S) and gum arabic (G) would be used to synthesize the sundew-inspired hydrogels, we then set out to determine their optimal ratios. To optimize the performance of the sundew-inspired

adhesive hydrogels, seven different candidate hydrogels were prepared according to different ratios of S/G (S1G1, 1:1; S1G2, 1:2; S1G3, 1:3; S2G1, 2:1; S2G3, 2:3; S3G1, 3:1; and S3G2, 3:2) and maintained at a total concentration of 4% (w/v). After adhesive performance comparison, S1G2, S2G1, and S1G1 were selected for further testing because of their superior adhesion strength compared to the other four S/G hydrogel ratios.  $\text{Ca}^{2+}$ , a divalent cation, was also included in the sundew-inspired hydrogel's synthesis because of its mediation of hydrogel assembly and modulation for wound contracture and closure. Varying concentrations of  $\text{Ca}^{2+}$ , 1, 5, 10, 15, 20, and 25 mM, were introduced to the sundew-inspired hydrogel that exhibited the strongest adhesion strength without the addition of  $\text{Ca}^{2+}$  (S1G1). Of the differential  $\text{Ca}^{2+}$  concentrations, 5, 10, and 15 mM were selected for further testing as candidate additions to the sundew-inspired hydrogel because of their superior adhesive strength. A detailed description of our approach to synthesize sundew-inspired hydrogels is outlined in Figure 1, and a summary of the chemical concentrations and code names for the sodium alginate, gum arabic, and typical sundew-inspired adhesive hydrogels is located in Table 1. The above experiments were critical to the optimization and synthesis of the sundew-inspired adhesive hydrogels. It was these studies that allowed us to select the best hydrogels for further testing as wound-healing therapeutics.

### Morphological, Physical, and Chemical Analysis of Sundew-Inspired Adhesive Hydrogels

The adhesion strength of gum arabic, sodium alginate, S1G2, S1G1, and S2G1 samples without  $\text{Ca}^{2+}$  are presented in Figure 2C. Adhesion strength of the S1G1 samples with 5, 10, and 15 mM  $\text{Ca}^{2+}$  are shown in Figure 2D. The differences in the adhesion strength showed that S1G1Ca10 was the best candidate hydrogel; however, all of the sundew-inspired candidate hydrogels had superior adhesion strength compared to that of gum arabic and sodium alginate alone. This could be due to the composition of the adhesive because the nanoparticles are instrumental for adhesive performance. We observed better mobility and higher deformation resistance in gum arabic nanoparticles, thus indicating that they may play an important role in increasing the internal cohesion strength of the sundew-inspired adhesive hydrogels.<sup>40,41</sup> Besides the nanoparticles' functions in strengthening the internal strength of the cohesion zone, gum arabic nanoparticles may contribute to the anisotropic nanostructures of the nanocomposite adhesive.

Our data demonstrated that without the addition of  $\text{Ca}^{2+}$  S1G1 had strongest adhesion strength compared to the other potential candidate hydrogels. This meant that in a 1:1 ratio of sodium alginate and gum arabic, the nanomorphology and chemical structure of the hydrogel is the best in terms of adhesive performance. Once we determined that a 1:1 ratio of sodium alginate to gum arabic had the best adhesive strength we then tested various  $\text{Ca}^{2+}$  concentrations with S1G1 to see which would best enhance the adhesive strength of the sundew-inspired adhesive hydrogels (Figure 2D). The sundew-inspired adhesive hydrogel with 10 mM  $\text{Ca}^{2+}$  (S1G1Ca10) had the highest adhesion strength compared to that of all other concentrations. In fact, the adhesion strength of S1G1Ca10 was almost triple that seen with gum arabic or sodium alginate. Of note, the hydrogel with the highest  $\text{Ca}^{2+}$  concentration, S1G1Ca15, had less adhesion strength than did S1G1Ca10, despite having more  $\text{Ca}^{2+}$ . The reduced strength observed in S1G1Ca15 might have resulted because of the formation of too many egg-box structures. If this was the case, then it would explain the

brittle properties observed in S1G1Ca15. Therefore, we found that the concentration of  $\text{Ca}^{2+}$  was not better at greater magnitudes but rather optimal at 10 mM when attempting to synthesize a sundew-inspired hydrogel with high levels of adhesion strength.

The surface morphology and complex 3D nano- and microstructures of gum arabic and S1G1Ca10 were also assessed using atomic force microscopy (AFM) (Figure 2A,B). AFM determined that the nanostructure of gum arabic was comprised of 50 nm nanoparticles, a result which is consistent with our dynamic light scattering (DLS) findings. The nanofibers in the sundew adhesive are believed to be linearly assembled by the nanoparticles in the sundew adhesive; therefore, the nanoparticles from gum arabic may provide similar assembly potential in the sundew-inspired adhesive hydrogels. Figure 2B shows the nanoparticles within the nanomorphological structure of the sundew-inspired adhesive hydrogel S1G1Ca10. Compared to S1G1Ca10, all other candidate hydrogels formed film structures without apparent networks. We observed that the sundew-inspired adhesive hydrogel's nanoparticle assembly into network structures was similar to that observed in the natural sundew adhesive assembly process. Given the analogy between the sundew-inspired and natural sundew hydrogels micro- and nanostructures, we hypothesized that application of our synthesized hydrogels to a wound site would help maintain a physiologically moist microenvironment that promotes healing and the formation of granulation tissue during the repair process.<sup>42</sup> Thus, the nanostructure's adhesive forces would have a "suturing" effect at the wounded site and enhance the wound's contracture and closure. These properties made the sundew-inspired hydrogel S1G1Ca10 an excellent candidate therapeutic to accelerate the wound-healing process.<sup>43,44</sup>

To evaluate further the force of the sundew-inspired adhesive hydrogels, the adhesive force of gum arabic, sodium alginate, S1G1, and S1G1Ca10 samples were measured by AFM (Figures 2E and S1). Interactions between the tip of cantilever and the samples were recorded as force measurements. With AFM strength measurements, the hydrogel was positioned on the coverslip in a state where force was absent at the interface. In this experiment, resistance force was induced when the cantilever contacted the sample, increased when the cantilever indented the sample, and decreased when the cantilever retracted. Thus, adhesive force was recorded at the end of the connection between cantilever tip and the sample and coincided with the lowest point in the force curve (Figure S1). We found that the room-temperature adhesive force of the sundew-inspired adhesive hydrogel S1G1Ca10 ( $165.7 \pm 10.3$  nN) was significantly greater than that from the control samples ( $26.3 \pm 8.2$  nN), gum arabic ( $62.4 \pm 11.1$  nN), sodium alginate ( $72.7 \pm 9.5$  nN), and S1G1 ( $123.3 \pm 9.2$  nN). Figure 2E summarizes the adhesive forces recorded for all samples and clearly indicates the significant difference observed between the sundew-inspired adhesive hydrogels S1G1Ca10 and all others. The high adhesion strength of S1G1Ca10 indicated that it might have the potential to function as a "glue", cementing the two skin margins together to enhance wound closure at the site of injury. Our results from the nanomorphology and adhesion strength experiments indicated that the sundew-inspired adhesive hydrogel S1G1Ca10 had the best adhesion strength among the sundew-inspired hydrogels and commercially available biomaterials.

The rheological behaviors of the different hydrogels were characterized and evaluated as a way to determine further which sundew-inspired adhesive hydrogel was the best candidate for wound-healing therapeutics. Measurement of viscosity as a function of the shear rate showed that the sundew-inspired adhesive hydrogels S1G1Ca10 and S1G1 had decreasing levels of viscosity with increasing shear rates (Figure 2F,G), a property known as shear-thinning behavior. The highest viscosity sample was S1G1Ca15; however, its low adhesion strength made it a poor hydrogel candidate. In S1G1Ca15, the molecular interactions between sodium alginate and gum arabic were decreased across the nanostructure, whereas the high level of  $\text{Ca}^{2+}$  mediated the formation of extensive egg-box structures, thus resulting in the acquisition of a brittle nanostructure and the subsequent suppression of cohesive forces between sodium alginate and gum arabic.

Besides S1G1Ca15, all the other candidate sundew-inspired hydrogels had similar variation trends in adhesion strength as determined by the lap shear tests and AFM force-curve measurements. Shear-thinning behavior is observed in biological fluids such as blood and biomaterials such as gelling products. Materials with shear-thinning behavior have high viscosity at low shear rates, thus adding properties of firmness, stability, and durability to products in which they are added.<sup>3</sup> Because shear rates increase as viscosity decreases, products with shear-thinning behaviors are absorbed easily into the skin with topical application. Moreover, the high adhesive strength of the sundew-inspired adhesive hydrogels made them an ideal synthetic bandage that remained on the skin following application. Sundew has a good viscoelastic property, which also balances the interacting force between flow and flow resistance. Features such as these make the sundew-inspired adhesive hydrogel S1G1Ca10 suitable for wound-healing applications. Fourier transform infrared spectroscopy (FTIR) was also used to observe peak shifts caused from the interactions between sodium alginate and gum arabic. The FTIR spectra in Figure S2 shows a typical spectral features of the sundew-inspired adhesive hydrogels compared to sodium alginate or gum arabic alone.

### **In Vitro Wound Closure, Fibroblast Stiffness, and Cytotoxicity Characterizations**

Cell migration is a rate-limiting event in the wound-healing process. Therefore, we examined how the hydrogels affected dermal fibroblast and epidermal keratinocyte migration during the wound induction and healing process. The scratch assay method was used in L929 dermal fibroblasts and HaCaT keratinocytes to evaluate wound closure in vitro. In fibroblasts, the sundew-inspired adhesive hydrogel S1G1Ca10 enhanced wound closure the most (~38%, Figure 3A) compared to all other hydrogels at the 6 h time point. This result was replicated in keratinocytes, where S1G1Ca10 enhanced wound closure the most (18%, Figure 3B). We observed different speeds of complete wound closure between the fibroblast and keratinocyte cell lines. Our result was in-line with the notion that in classical wound healing keratinocytes migration to the site of injury is secondary to dermal fibroblast infiltration.<sup>45</sup> Thus, by 24 h, we observed complete wound closure of L929 fibroblasts treated with S1G1Ca10, and in keratinocytes this result was observed at 48 h. Of note is that S1G1Ca10 enhanced the rate of wound closure significantly faster in both cell lines compared to all other samples (control, sodium alginate, gum arabic, and S1G1). Differences between the percent of wound closure and speed of wound closure observed with S1G1 and

S1G1Ca10 treatment was likely due to the addition of  $\text{Ca}^{2+}$  in S1G1Ca10. Recent advances using keratinocytes, dermal fibroblasts, and reconstructed epidermis organ cultures have shown that local  $\text{Ca}^{2+}$  levels speed up the wound-healing process by modulating cell proliferation, maturation, and the creation of epidermal lipid barriers. Thus, in vitro, the sundew-inspired adhesive hydrogel S1G1Ca10 proved to be a superior biomaterial that can accelerate the wound-healing process.

Cell stiffness is an important biomarker for cell migration. It has been demonstrated that cells with higher migratory potential are less stiff than those with lower migratory potential.<sup>46</sup> Moreover, previous studies have suggested that fibroblast cells can modify their internal stiffness to direct cell migration and wound repair.<sup>47</sup> We measured the stiffness of single fibroblasts treated with different hydrogels (sodium alginate, gum arabic, S1G1, and S1G1Ca10) for 6 and 24 h using AFM (Figure 3C,D). The control group, untreated fibroblasts, were significantly stiffer than all other samples, indicating that the sundew-inspired adhesive hydrogels could decrease fibroblast stiffness. This observed decrease in stiffness could subsequently enhance their motility and thus migration to the site of injury. The cytotoxicity of control, gum arabic, sodium alginate, S1G1, and S1G1Ca10 were also investigated in L929 fibroblast (Figure 3E) and HaCaT keratinocytes (Figure 3F). No cytotoxicity was observed in L929 and HaCaT cells treated with hydrogels when compared to the untreated controls. These combined results demonstrated that the sundew-inspired adhesive hydrogel S1G1Ca10 was a safe and effective means to modulate fibroblast stiffness and cell migration following injury in vitro.

### In Vivo Wound Closure Studies

The wound-healing process involves three overlapping stages: the inflammatory stage, the proliferative stage, and the remodeling phase.<sup>48</sup> The inflammatory phase includes the establishment of homeostasis, the prevention of further blood loss, and the influx of inflammatory cells to the site of injury. The second phase, the proliferative phase, is characterized by granulation formation, fibrogenesis, neovascularization, wound contraction, and re-epithelialization. In the final and potentially most important phase, remodeling, a mass of collagen and extracellular matrix proteins persist at the site of injury to determine the strength and appearance of the scar that has formed.

To assess the in vivo wound-healing efficacy of the sundew-inspired adhesive hydrogels, full thickness skin incisions were made on the backs of mice. After injury, different biomaterials were topically applied to the wound sites. Figure 4A (left) shows images of the wounds taken at different time intervals after treating the mice without (control) or with sodium alginate, gum arabic, S1G1, and S1G1Ca10. There was no sign of inflammation or infection following hydrogel application to the wound area. Furthermore, the growth of new epidermis extended to the center of all hydrogel treated wounds, resulting in a reduction in wounded area. Among all hydrogel treatment groups, wound contraction was most accelerated during the first 11 days in mice treated with S1G1Ca10 (Figure 4A, right). At four days following wound induction, the wound closure rate of S1G1Ca10 reached 62%, which was significantly higher than that of all other treatments (control, 24%; sodium alginate, 41%; gum arabic, 31%; and S1G1, 42%). This result might have been attributed to the adhesion

strength, shear-thinning viscosity, and nanomorphological structure of the sundew-inspired adhesive hydrogel S1G1Ca10. The properties of this hydrogel could have resulted in maintenance of a physiologically moist microenvironment. Accordingly, this would provide a “suturing” effect at the wound site, thus enhancing wound contraction and closure during the early stage of the wound-healing process.

Histological examination of the wounds with or without hydrogel treatment was examined on the 11th postoperative day (Figure 4B). The surface of the wounds treated with the sundew-inspired adhesive hydrogel S1G1Ca10 showed complete formation of a new epithelium (Figure 4B, first row, H&E samples). Collagen, a predominant structural protein in skin, is necessary to reconstruct dermal tissue at wound sites effectively. Eleven days after the incisions were induced, tissues were also stained with Masson’s trichrome to identify collagen deposition (Figure 4B, second row). A more intense blue color was observed in the wounded tissue covered with S1G1Ca10, indicating that collagen deposition was most enhanced in S1G1Ca10 compared to the other samples. We also observed that the S1G1Ca10-treated wounds had more densely packed collagen fibers running in parallel arrangement and more collagen fiber accumulation in the extracellular matrix. Compared to S1G1Ca10, the other samples appeared to have loosely packed collagen fibers running in irregular arrangements. To determine if local hydrogel administered had accumulated in different organs or induced unexpected toxicities, we performed H&E histological evaluation on the brain, heart, liver, lung, kidney, and spleen of each animal at day 11 (Figure S3). Examination of the H&E stained organs revealed no significant signs of toxicity, thus supporting the use of the sundew-inspired adhesive hydrogels for wound-healing applications. We also performed ELISAs on the serum samples of the mice to determine if there were any observable inflammatory effects following sundew-inspired adhesive hydrogel treatment. Again, no detectable changes in pro-inflammatory cytokines TNF- $\alpha$  and IL-6 were observed at day 11 in the animal serum (Figure S4). Serum LDH levels, which can be used as a marker for tissue injury, were also within normal range and did not differ between treatment or control groups. Following the conclusion of these *in vivo* studies, our findings demonstrated that sundew-inspired adhesive hydrogels are safe and biocompatible therapies for wound-healing applications.

### Isolation and Characterization of ADSCs

We then set out to determine if ADSCs could be used in combination with sundew-inspired hydrogels to enhance further the wound-healing process. ADSCs are characterized by high viability, the ability to undergo adipogenic differentiation, adherence to culture plates, acquisition of fibroblast morphology, and specific cell-surface markers (CD73<sup>+</sup> CD105<sup>+</sup> CD31<sup>-</sup> CD45<sup>-</sup>). Mechanical and enzymatic techniques were used to isolate ADSCs from mice. *In vitro*, the ADSCs proliferated rapidly and formed a homogeneous monolayer with fibroblastlike morphology (Figure 5A). Flow cytometry confirmed that the isolated cells were in fact ADSCs (Figure 5C) because cells were positive for mesenchymal surface markers (CD73 and CD105) and negative for endothelial (CD31) and hematopoietic (CD45) markers. Following confirmation that the isolated cells were ADSCs, we investigated whether or not the cells could undergo adipogenic differentiation in the absence or presence of sundew-inspired or -derived hydrogels. Culture plates were left unmodified or coated with

the hydrogels, and ADSCs were then induced with adipogenic medium. The presence of adipocytes was identified by Oil Red O staining (Figure 5B), and our results showed that all groups demonstrated apparent differentiation. No noticeable differences in adipocyte differentiation were observed between conditions. Our results suggested that sundew-derived and -inspired adhesive hydrogels did not suppress the adipogenic potential of ADSCs. Thus, the hydrogels could function as scaffolds capable of supporting the functionalities of ADSCs at sites of cutaneous injury.

### Evaluation of Sundew-Derived and -Inspired Adhesive Hydrogels Combined with ADSCs

We compared sundew-derived and -inspired adhesive hydrogels, with or without ADSCs, against a commercial hydrogel, mucin, and cellulose (Figure 6) to determine if hydrogel-ADSC combination therapy had superior wound-healing effects. Similar to our first in vivo experiments, skin incisions were made on the back of mice. Under ADSC conditions, 50  $\mu\text{L}$  of ADSCs suspended in culture medium ( $1 \times 10^6$  cells per total volume) were pipetted onto the wounded area. Under all conditions,  $\sim 100 \mu\text{L}$  of hydrogel, mucin, or cellulose was then topically applied. Of note is that the effects of ADSC were always investigated in combination with hydrogels rather than alone because there was then no way to contain the cells and maintain their viability without the “suturing” effects of the hydrogels. If we had investigated their effects alone, then invasive methods such as injection, engraftment, or suture would have been required and could have confounded the wound-healing results. Mice treated with sundew-derived or -inspired adhesive hydrogels exhibited similar wound closure rates, and the addition of ADSCs further accelerated the processes. Head-to-head comparison between all groups demonstrated that the combination therapy of ADSC and sundew-derived or -inspired hydrogels was superior for enhancing healing. Earlier work has extensively shown that cellulose, sodium alginate, and gum arabic have wound-healing applications. Our data showed that sundew-inspired adhesive hydrogels have advantages over mucin (Figure 6A), sodium alginate, and gum arabic. It could be that sundew-inspired and -derived hydrogels provide a moisture-rich microenvironment that is beneficial to the survival, proliferation, and differentiation of cells involved in the rehabilitation of wound sites. H&E stained sections of the wounded skins treated with sundew-derived and -inspired adhesive hydrogels after 11 days (Figure 6B) demonstrated that wounds treated with these hydrogels have a markedly higher rehabilitation rate compared to that of untreated groups. Similar to our earlier in vivo toxicity studies, the H&E organ staining (brain, heart, liver, lung, kidney, and spleen) for all groups showed no pathological changes (Figure S5). That finding further supported the biocompatibility of ADSC/sundew-inspired adhesive hydrogel combination therapy for wound-healing applications.

## CONCLUSIONS

Although stem-cell-based therapies have been used in conjunction with hydrogel therapeutics in the past, this is to our knowledge the first time that the combination of ADSCs and sundew-inspired hydrogels has been successfully implemented as a combination therapy to accelerate the wound-repair process. One caveat to natural hydrogel therapy has been the limited ability to acquire sufficient biomaterials for mass production; however, our work demonstrated the efficacy and limited toxicity of using sundew-inspired adhesive

hydrogels in combination with ADSCs as a novel wound-healing application that overcomes some of the synthesis and optimization challenges faced by other hydrogels. The sundew-inspired adhesive hydrogels had moderate adhesive strength, unique nanomorphology, promising biocompatibility, and good viscosity properties that made them ideal therapeutic agents. Intrinsically, and with the aid of ADSCs, sundew-inspired hydrogels promoted wound healing. The *in vitro* and *in vivo* experimental wound-closure data showed that sundew-derived and -inspired adhesive hydrogels both significantly enhance wound re-epithelialization, collagen deposition, and contraction. Furthermore, the combination had preferable wound-healing abilities compared to that of naturally occurring cellulose, mucin, and a commercially available wound-healing hydrogel. Accordingly, our biosynthetic strategy demonstrates how inspiration from nature can be recreated in the laboratory to synthesize novel therapeutics that promote regeneration and wound healing without encountering the limitations of bioavailability.

## Supplementary Material

Refer to Web version on PubMed Central for supplementary material.

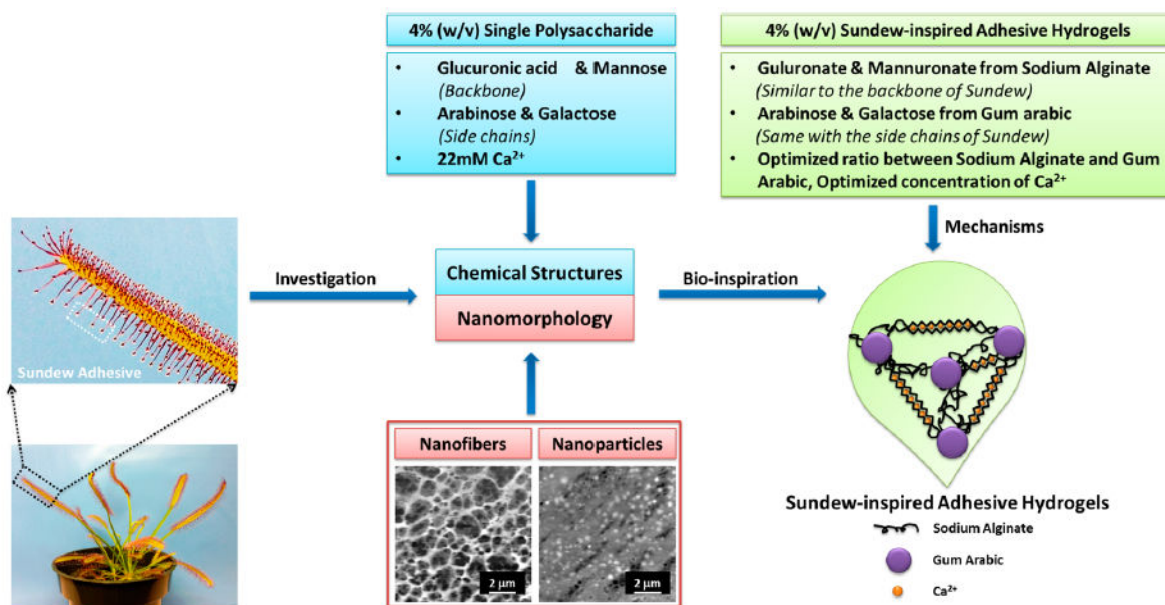
## References

1. Guo S, DiPietro LA. Factors Affecting Wound Healing. *J Dent Res*. 2010; 89(3):219–229. [PubMed: 20139336]
2. Li Y, Cheng Y, Xu T. Design, Synthesis and Potent Pharmaceutical Applications of Glycodendrimers: A Mini Review. *Curr Drug Discovery Technol*. 2007; 4(4):246–254.
3. Maalej H, Moalla D, Boisset C, Bardaa S, Ayed HB, Sahnoun Z, Rebai T, Nasri M, Hmidet N. Rheological, Dermal Wound Healing and *in vitro* Antioxidant properties of Exopolysaccharide Hydrogel from *Pseudomonas Stutzeri* AS22. *Colloids Surf B*. 2014; 123(0):814–824.
4. Wen Y, Liu W, Bagia C, Zhang S, Bai M, Janjic JM, Giannoukakis N, Gawalt ES, Meng WS. Antibody-functionalized Peptidic Membranes for Neutralization of Allogeneic Skin Antigen-presenting Cells. *Acta Biomater*. 2014; 10(11):4759–4767. [PubMed: 25117952]
5. Calvert P. Hydrogels for Soft Machines. *Adv Mater*. 2009; 21(7):743–756.
6. Wu J, Wu D, Mutschler MA, Chu C-C. Cationic Hybrid Hydrogels from Amino-Acid-Based Poly(ester amide): Fabrication, Characterization, and Biological Properties. *Adv Funct Mater*. 2012; 22(18):3815–3823.
7. Wen Y, Kolonich HR, Kruszewski KM, Giannoukakis N, Gawalt ES, Meng WS. Retaining Antibodies in Tumors with a Self-Assembling Injectable System. *Mol Pharmaceutics*. 2013; 10(3): 1035–1044.
8. Li Y, Zhang W-B, Hsieh IF, Zhang G, Cao Y, Li X, Wesdemiotis C, Lotz B, Xiong H, Cheng SZD. Breaking Symmetry toward Nonspherical Janus Particles Based on Polyhedral Oligomeric Silsesquioxanes: Molecular Design, “Click” Synthesis, and Hierarchical Structure. *J Am Chem Soc*. 2011; 133(28):10712–10715. [PubMed: 21682260]
9. Mohamed A, Xing M. Nanomaterials and Nanotechnology for Skin Tissue Engineering. *Int J Burns Trauma*. 2012; 2(1):29–41. [PubMed: 22928165]
10. Hong H-J, Jin S-E, Park J-S, Ahn WS, Kim C-K. Accelerated Wound Healing by smad3 Antisense Oligonucleotides-impregnated Chitosan/alginate Polyelectrolyte Complex. *Biomaterials*. 2008; 29(36):4831–4837. [PubMed: 18829100]
11. Murakami K, Aoki H, Nakamura S, Nakamura S-i, Takikawa M, Hanzawa M, Kishimoto S, Hattori H, Tanaka Y, Kiyosawa T, Sato Y, Ishihara M. Hydrogel Blends of Chitin/ chitosan, Fucoidan and Alginate as Healing-impaired Wound Dressings. *Biomaterials*. 2010; 31(1):83–90. [PubMed: 19775748]



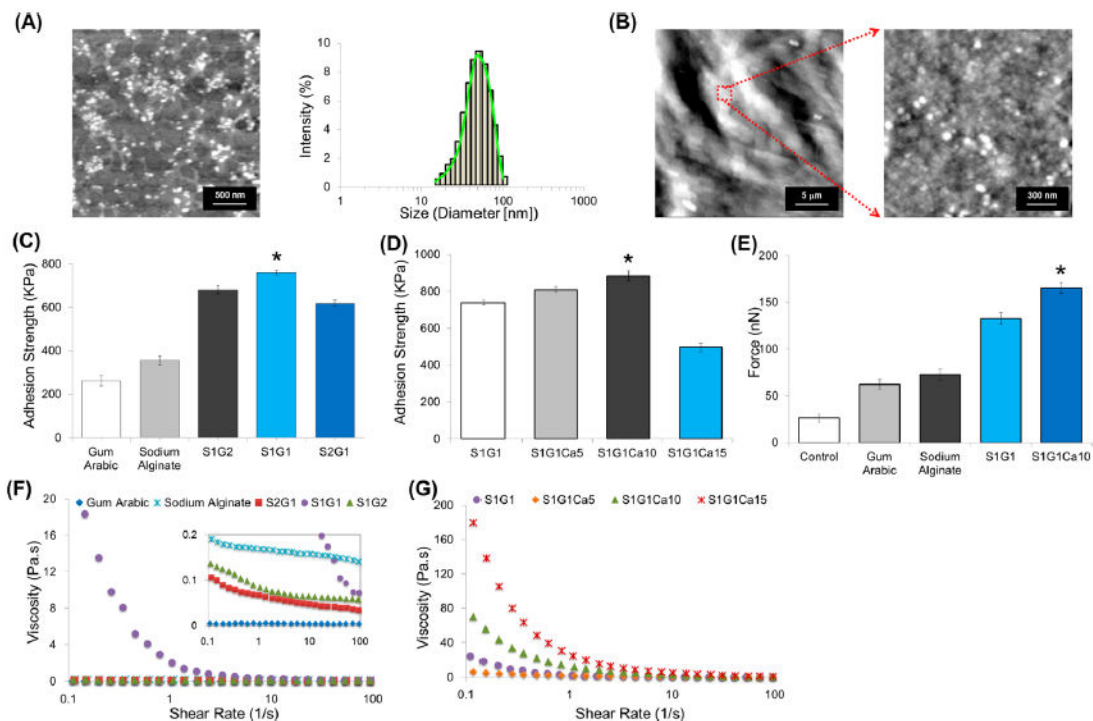
12. Lin J, Li C, Zhao Y, Hu J, Zhang L-M. Co-electrospun Nanofibrous Membranes of Collagen and Zein for Wound Healing. *ACS Appl Mater Interfaces*. 2012; 4(2):1050–1057. [PubMed: 22242622]
13. Elsner JJ, Shefy-Peleg A, Zilberman M. Novel Biodegradable Composite Wound Dressings with Controlled Release of Antibiotics: Microstructure, Mechanical and Physical Properties. *J Biomed Mater Res Part B*. 2010; 93B(2):425–435.
14. Zhang M, Lenaghan S, Xia L, Dong L, He W, Henson W, Fan X. Nanofibers and Nanoparticles from the Insect-capturing Adhesive of the Sundew (*Drosera*) for Cell Attachment. *J Nanobiotechnol*. 2010; 8(1):20.
15. Li X, Hu A, Ye L. Structure and Property of Porous Polyvinylalcohol Hydrogels for Microorganism Immobilization. *J Polym Environ*. 2011; 19(2):398–404.
16. Huang Y, Wang Y, Sun L, Agrawal R, Zhang M. Sundew Adhesive: A Naturally Occurring Hydrogel. *J R Soc Interface*. 2015; 12(107)
17. Lenaghan SC, Serpersu K, Xia L, He W, Zhang M. A Naturally Occurring Nanomaterial from the Sundew (*Drosera*) for Tissue Engineering. *Bioinspiration Biomimetics*. 2011; 6(4):046009. [PubMed: 22064887]
18. Crouch IJ, Finnie JF, van Staden J. Studies on the Isolation of Plumbagin from *in vitro* and *in vivo* Grown *Drosera* Species. *Plant Cell, Tissue Organ Cult*. 1990; 21(1):79–82.
19. Jayaram K, Prasad MNV. Rapid *in vitro* Multiplication of *Drosera Indica* L.: a Vulnerable, Medicinally important Insectivorous Plant. *Plant Biotechnol Rep*. 2007; 1(2):79–84.
20. Rost K, Schauer R. Physical and Chemical Properties of the Mucin secreted by *Drosera capensis*. *Phytochemistry*. 1977; 16(9):1365–1368.
21. Gowda DC, Reuter G, Schauer R. Structural Studies of An Acidic Polysaccharide from the Mucin secreted by *Drosera capensis*. *Carbohydr Res*. 1983; 113(1):113–124.
22. Gombotz WR, Wee S. Protein Release from Alginate Matrices. *Adv Drug Delivery Rev*. 1998; 31(3):267–285.
23. Pawar SN, Edgar KJ. Alginate Derivatization: A Review of Chemistry, Properties and Applications. *Biomaterials*. 2012; 33(11):3279–3305. [PubMed: 22281421]
24. Samy WM, Ghoneim AI, Elgindy NA. Novel Microstructured Sildenafil Dosage forms as Wound Healing Promoters. *Expert Opin Drug Delivery*. 2014; 11(10):1525–1536.
25. Ali BH, Ziada A, Blunden G. Biological effects of Gum Arabic: A Review of Some Recent Research. *Food Chem Toxicol*. 2009; 47(1):1–8. [PubMed: 18672018]
26. Clark DT, Gazi MI, Cox SW, Eley BM, Tinsley GF. The Effects of Acacia Arabica Gum on the *in vitro* Growth and Protease Activities of Periodontopathic Bacteria. *J Clin Periodontol*. 1993; 20(4): 238–243. [PubMed: 8473532]
27. Lansdown ABG. Calcium: A Potential Central Regulator in Wound Healing in the Skin. *Wound Repair Regen*. 2002; 10(5):271–285. [PubMed: 12406163]
28. Lee SH, Elias PM, Proksch E, Menon GK, Mao-Qiang M, Feingold KR. Calcium and Potassium are Important Regulators of Barrier Homeostasis in Murine Epidermis. *J Clin Invest*. 1992; 89(2): 530–538. [PubMed: 1737844]
29. Dlugosz AA, Yuspa SH. Protein Kinase C Regulates Keratinocyte Transglutaminase (TGK) Gene Expression in Cultured Primary Mouse Epidermal Keratinocytes Induced to Terminally Differentiate by Calcium. *J Invest Dermatol*. 1994; 102(4):409–414. [PubMed: 7908680]
30. Magee AI, Lytton NA, Watt FM. Calcium-induced Changes in Cytoskeleton and Motility of Cultured Human Keratinocytes. *Exp Cell Res*. 1987; 172(1):43–53. [PubMed: 2443374]
31. Cao Y, Sun Z, Liao L, Meng Y, Han Q, Zhao RC. Human Adipose Tissue-derived Stem Cells Differentiate into Endothelial Cells *in vitro* and Improve Postnatal Neovascularization *in vivo*. *Biochem Biophys Res Commun*. 2005; 332(2):370–379. [PubMed: 15896706]
32. Rigotti G, Marchi A, Galie M, Baroni G, Benati D, Krampera M, Pasini A, Sbarbati A. Clinical Treatment of Radiotherapy Tissue Damage by Lipoaspirate Transplant: A Healing Process Mediated by Adipose-Derived Adult Stem Cells. *Plast Reconstr Surg*. 2007; 119(5):1409–1422. [PubMed: 17415234]
33. Gimble JM, Katz AJ, Bunnell BA. Adipose-Derived Stem Cells for Regenerative Medicine. *Circ Res*. 2007; 100(9):1249–1260. [PubMed: 17495232]

34. González MA, Gonzalez-Rey E, Rico L, Büscher D, Delgado M. Adipose-Derived Mesenchymal Stem Cells Alleviate Experimental Colitis by Inhibiting Inflammatory and Autoimmune Responses. *Gastroenterology*. 2009; 136(3):978–989. [PubMed: 19135996]
35. Kim W-S, Park B-S, Sung J-H, Yang J-M, Park S-B, Kwak S-J, Park J-S. Wound Healing Effect of Adipose-derived Stem Cells: A Critical Role of Secretory Factors on Human Dermal Fibroblasts. *J Dermatol Sci*. 2007; 48(1):15–24. [PubMed: 17643966]
36. Lee EY, Xia Y, Kim W-S, Kim MH, Kim TH, Kim KJ, Park BS, Sung JH. Hypoxia-enhanced Wound-healing Function of Adipose-derived Stem Cells: Increase in Stem Cell Proliferation and up-regulation of VEGF and bFGF. *Wound Repair Regen*. 2009; 17(4):540–547. [PubMed: 19614919]
37. Strem BM, Hicok KC, Zhu M, Wulur I, Alfonso Z, Schreiber RE, Fraser JK, Hedrick MH. Multipotential Differentiation of Adipose Tissue-derived Stem Cells. *Keio J Med*. 2005; 54(3): 132–141. [PubMed: 16237275]
38. Mizuno H. Adipose-derived Stem Cells for Tissue Repair and Regeneration: Ten Years of Research and A Literature Review. *J Nippon Med Sch*. 2009; 76(2):56–66. [PubMed: 19443990]
39. Vichare S, Sen S, Inamdar MM. Cellular Mechanoadaptation to Substrate Mechanical Properties: Contributions of Substrate Stiffness and Thickness to Cell Stiffness Measurements using AFM. *Soft Matter*. 2014; 10(8):1174–1181. [PubMed: 24651595]
40. Sun L, Yi S, Wang Y, Pan K, Zhong Q, Zhang MA. Bio-inspired Approach for in situ Synthesis of Tunable Adhesive. *Bioinspiration Biomimetics*. 2014; 9(1):016005. [PubMed: 24343277]
41. Kutvonen A, Rossi G, Puisto SR, Rostedt NKJ, Ala-Nissila T. Influence of Nanoparticle size, Loading, and Shape on the Mechanical Properties of Polymer Nanocomposites. *J Chem Phys*. 2012; 137(21):214901. [PubMed: 23231257]
42. Motta GJ. Calcium Alginate Topical Wound Dressings: A New Dimension in the Cost-effective Treatment for Exudating Dermal Wounds and Pressure Sores. *Ostomy Wound Manag*. 1989; 25:52–56.
43. Wang Y, Yi S, Sun L, Huang Y, Zhang M. Charge-selective Fractions of Naturally Occurring Nanoparticles as Bioactive Nano-carriers for Cancer Therapy. *Acta Biomater*. 2014; 10(10):4269–4284. [PubMed: 24952072]
44. Wang Y, Sun L, Yi S, Huang Y, Lenaghan SC, Zhang M. Naturally Occurring Nanoparticles from *Arthrobotrys oligospora* as a Potential Immunostimulatory and Antitumor Agent. *Adv. Funct Mater*. 2013; 23(17):2175–2184.
45. Gurtner GC, Werner S, Barrandon Y, Longaker MT. Wound Repair and Regeneration. *Nature*. 2008; 453(7193):314–321. [PubMed: 18480812]
46. Swaminathan V, Mythreye K, O'Brien ET, Berchuck A, Blobe GC, Superfine R. Mechanical Stiffness Grades Metastatic Potential in Patient Tumor Cells and in Cancer Cell Lines. *Cancer Res*. 2011; 71(15):5075–5080. [PubMed: 21642375]
47. Solon J, Levental I, Sengupta K, Georges PC, Janmey PA. Fibroblast Adaptation and Stiffness Matching to Soft Elastic Substrates. *Biophys J*. 2007; 93(12):4453–4461. [PubMed: 18045965]
48. Arul V, Kartha R, Jayakumar R. A Therapeutic approach for Diabetic Wound Healing using Biotinylated GHK incorporated Collagen Matrices. *Life Sci*. 2007; 80(4):275–284. [PubMed: 17049946]



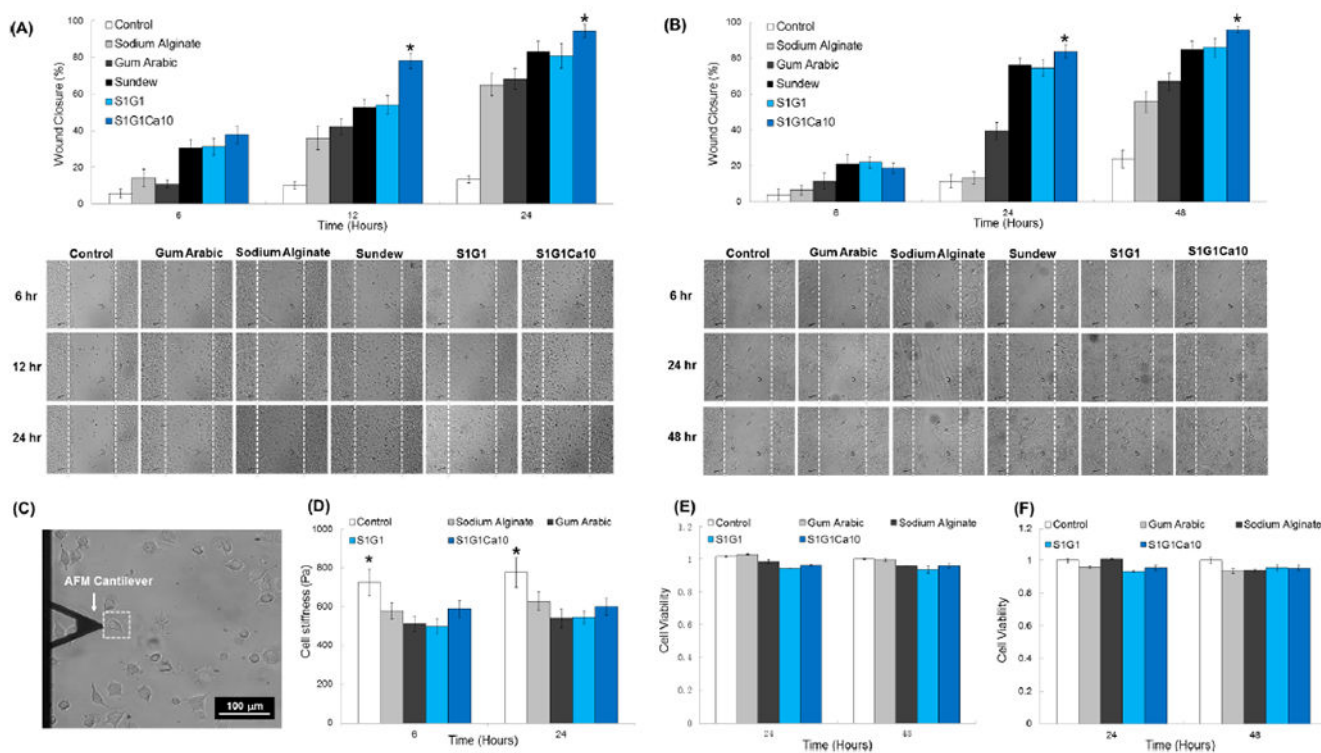
**Figure 1.**

Schematic of the sundew-inspired adhesive hydrogels from chemical structures and nanomorphology of the natural sundew adhesive. The 4% (w/v) single polysaccharide of sundew adhesive is composed of glucuronic acid and mannose as the backbone, arabinose and galactose as the side chains, and 22 mM  $\text{Ca}^{2+}$ . The scale bars in the AFM images of nanofibers and nanoparticles of the sundew adhesive are 2  $\mu\text{m}$ . The concentrations of the sundew-inspired adhesive hydrogels are defined as 4% (w/v), which is identical to that of the sundew adhesive hydrogels and makes them an excellent candidate for tissue engineering and regenerative medicine. Sodium alginate and gum arabic are selected as the polysaccharides to construct the main structure of the sundew-inspired adhesive hydrogels. The two polysaccharides have analogical structures to the backbones and side chains of the sundew adhesive polysaccharide. The divalent cations such as  $\text{Ca}^{2+}$  not only involve in the assembly processes of the sundew-inspired hydrogels through egg-box structure but also act as the modulator for wound contraction and closure. The sundew-inspired adhesive hydrogels are synthesized through the optimization of ratios between sodium alginate and gum arabic and concentrations of  $\text{Ca}^{2+}$ .



**Figure 2.**

Sundew-inspired hydrogels have superior adhesion strength, force, and resistance to shearing in vitro. Morphology, adhesive, and viscosity properties were examined in sundew-inspired adhesive hydrogels with and without  $\text{Ca}^{2+}$  as well as gum arabic and sodium alginate. (A) AFM image and DLS analysis of nanoparticles from gum arabic. The scale bar is 500 nm. The average size of the nanoparticles from gum arabic measured from AFM and DLS is around 50 nm. (B) Nanomorphological structure from the sundew-inspired adhesive hydrogels S1G1Ca10; the nano- and microenvironments are composed of nanoparticles. The scale bars are 5  $\mu\text{m}$  (left) and 300 nm (right). The nanomorphology of sundew-inspired adhesive hydrogels is analogous to that of the sundew-derived adhesive hydrogels. (C) Adhesion strength of sodium alginate, gum arabic, S1G2, S1G1, and S2G1 samples without  $\text{Ca}^{2+}$ . (D) Adhesion strength of the S1G1 samples with 5 (S1G1Ca5), 10 (S1G1Ca10), and 15 mM (S1G1Ca15)  $\text{Ca}^{2+}$ . (E) Adhesive forces of different samples measured by AFM. Error bars indicate SD. Significant differences between sample means are indicated; \*,  $P < 0.05$ . Both the lap-shear adhesion tests and AFM measurements indicate that the sundew-inspired adhesive hydrogels have the best adhesive performance. (F) Viscosity of the sodium alginate, gum arabic, S2G1, S1G1, and S1G2 samples without  $\text{Ca}^{2+}$ . (G) Viscosity of the S1G1 samples with 5 (S1G1Ca5), 10 (S1G1Ca10), and 15 mM (S1G1Ca15)  $\text{Ca}^{2+}$ . A shear-thinning behavior of the sundew-inspired adhesive hydrogels S1G1Ca10 is characterized by decreasing viscosity with increasing shear rate.

**Figure 3.**

Sundew-inspired hydrogels enhance wound closure without altering cell viability in vitro. Characterizations of in vitro scratch assays and cytotoxicity for L929 dermal fibroblasts and HaCaT keratinocytes as well as cell stiffness for L929 dermal fibroblasts. (A) Extent of wound closure in scratch assays of fibroblasts after different times and representative time-lapse images of scratch assays treated by control, gum arabic, sodium alginate, sundew-derived adhesive hydrogels, and sundew-inspired hydrogels (S1G1 and S1G1Ca10). (B) Extent of wound closure in scratch assays of keratinocytes after different times and representative time-lapse images of scratch assays treated by control, gum arabic, sodium alginate, sundew-derived adhesive hydrogels, S1G1, and S1G1Ca10. The results show that the L929 fibroblasts effect wound closure more rapidly than HaCaT keratinocytes. The sundew-inspired adhesive hydrogel S1G1Ca10 enhanced the rate of wound closure significantly in both L929 fibroblasts and HaCaT keratinocytes cell lines compared to other samples including control, sodium alginate, gum arabic, sundew-derived adhesive hydrogels, and S1G1. (C) Stiffness measurement of single cells (white dashed box) by AFM cantilever. The scale bar is 100  $\mu\text{m}$ . (D) Stiffness of fibroblast cells after 6 and 24 h of treatment by control, sodium alginate, gum arabic, S1G1, and S1G1Ca10. All of the hydrogel treatments decreased the stiffness of the fibroblast cells compared to that of the untreated control cells, indicating that adhesive hydrogels may promote cell motility and migration by reducing the stiffness of fibroblasts. Cytotoxicity measurements of control, gum arabic, sodium alginate, and the sundew-inspired adhesive hydrogels on (E) L929 fibroblasts and (F) HaCaT keratinocytes indicated that no treatments decreased cell viability. The result shows that sundew-inspired adhesive hydrogels are highly biocompatible materials with no demonstrated cytotoxicity against L929 fibroblasts or HaCaT keratinocytes. Bar graphs

represent mean  $\pm$  SD. Significant differences between sample means are indicated;\*,  $P < 0.05$ .

Author Manuscript

Author Manuscript

Author Manuscript

Author Manuscript

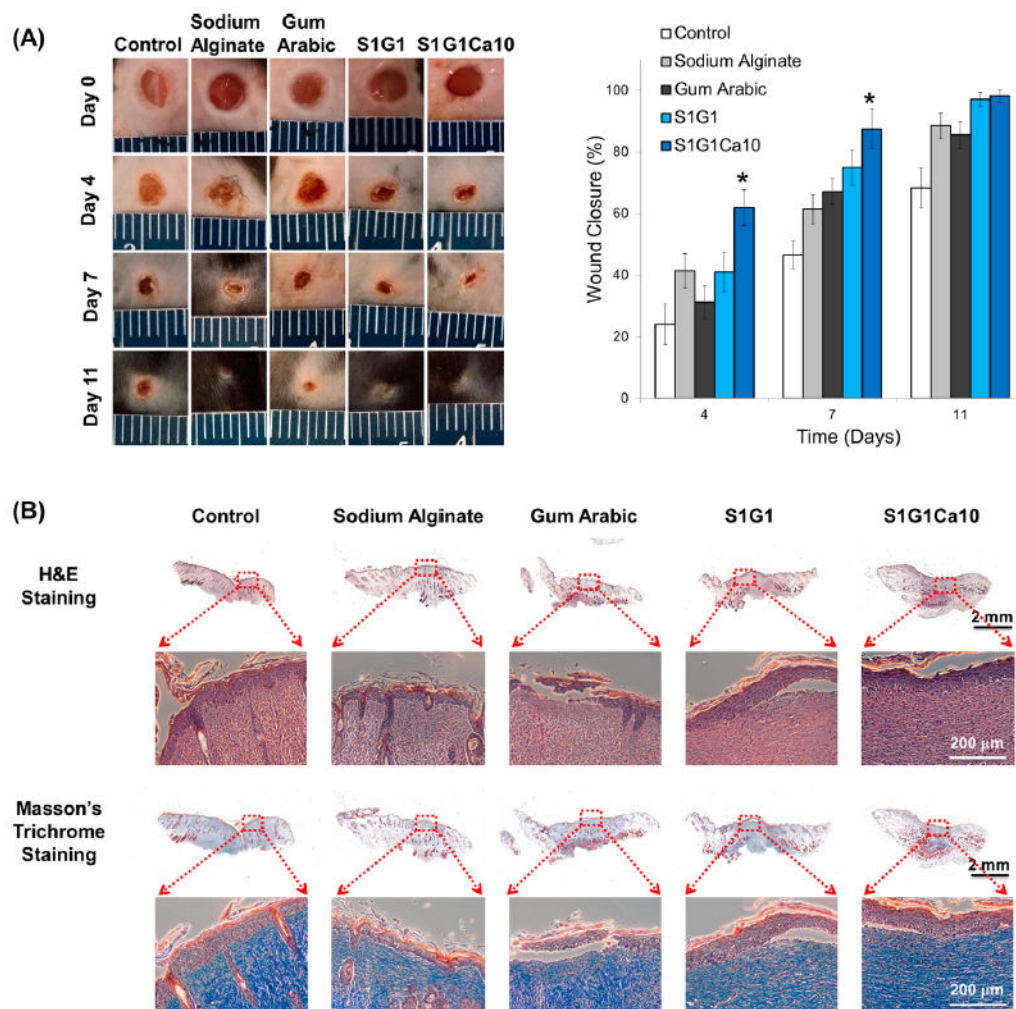


**Figure 4.** Sundew-inspired hydrogel S1G1Ca10 enhances wound closure in vivo. Results of in vivo wound-healing studies and histological analysis for control, sodium alginate, gum arabic, S1G1, and S1G1Ca10 samples. (A) Photographs of excised wound and quantitative evaluation of wound healing by calculating wound closure rate at day 0, 4, 7, and 11 of six mice in each group. Error bars indicate SD. Significant differences between sample means are indicated; \*,  $P < 0.05$ . The result shows that the growth of new epidermis is extended to the wound centers in all treated wound lesions, resulting in the reduced area of the wounds. Among the treatment groups, sundew-inspired adhesive hydrogel S1G1Ca10 enhances wound closure for up to 11 days as compared to control, sodium alginate, gum arabic, and S1G1. (B) Images of H&E stained and Masson's trichrome stained histological sections after 11 days of wound healing. The results indicate that the bioinspired adhesive hydrogels S1G1Ca10 significantly enhance wound re-epithelialization, collagen deposition, and wound closure.

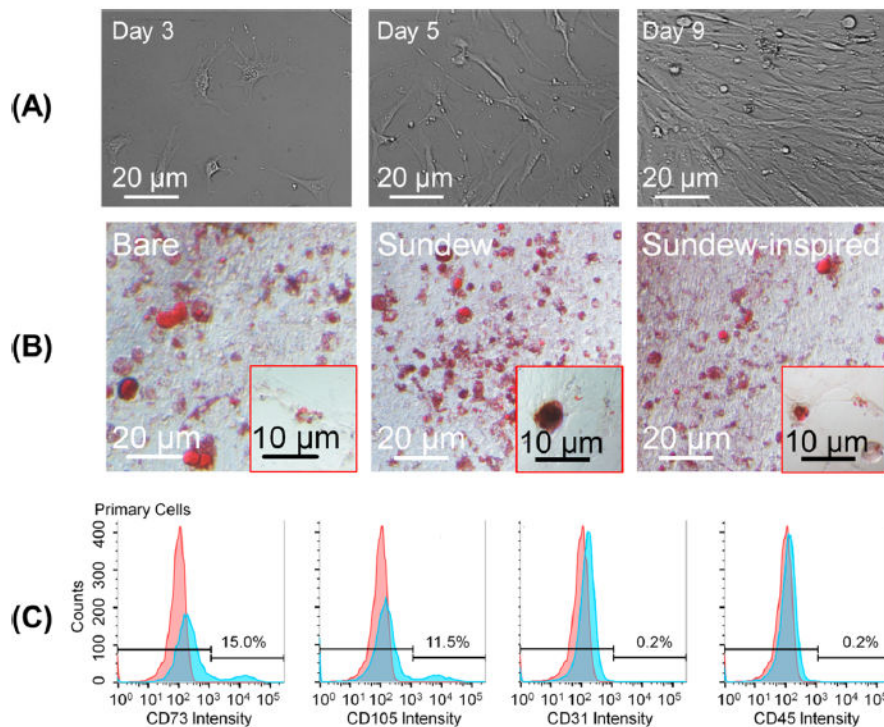


**Figure 5.**

Characterization of isolated ADSCs. Morphological observations, Oil Red O staining, and flow cytometry were used to characterize isolated ADSCs. (A) Morphological changes in isolated primary ADSCs on lysine-coated culture plates over time. The ADSCs proliferated rapidly in vitro, forming a homogeneous composition in monolayer, with fibroblastlike morphology. (B) ADSCs were plated onto bare culture plates or culture plates modified with sundew-inspired or -derived hydrogels and then induced with adipocyte differentiation medium. On day 7, cells were stained with Oil Red O. The result suggested that the sundew and sundew-inspired adhesive hydrogels do not suppress the differentiation of ADSC and thus are capable of acting as scaffolds that support the functionalities of ADSCs on wound sites. (C) Characterization of isolated ADSCs by determining expression level of CDs on the cytoplasmic membrane using flow cytometry. The ADSCs were positive for mesenchymal markers CD73 and CD105 and negative for endothelial marker CD31 and hematopoietic markers CD45, indicating that they are pluripotent.



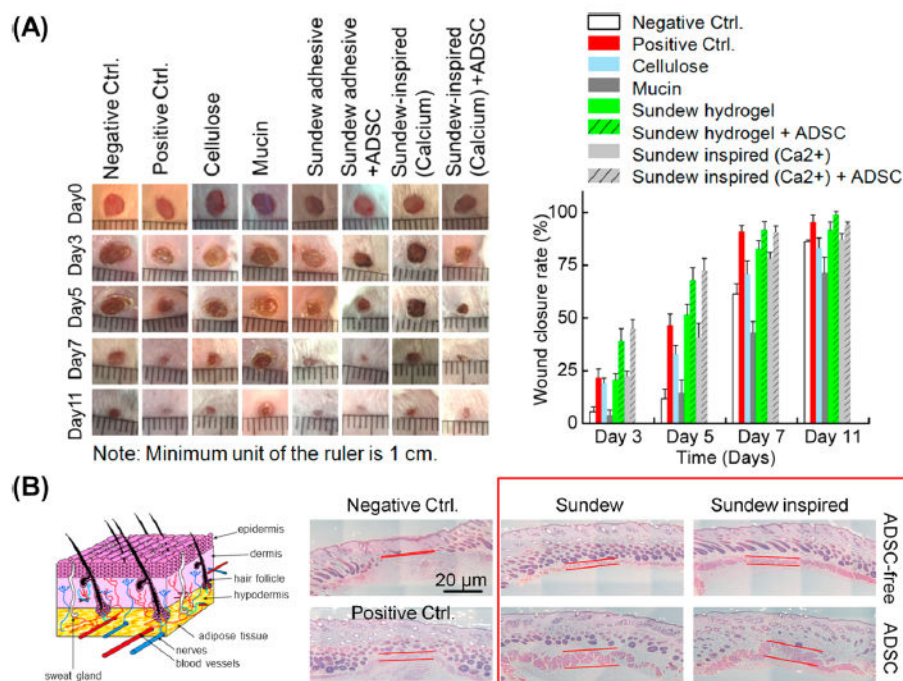


**Figure 6.**

Combination treatment with sundew-inspired adhesive hydrogels and ADSC accelerates initial wound closure in vivo. Sundew-derived and -inspired adhesive hydrogels seeded with or without ADSCs were evaluated and compared to naturally occurring cellulose and mucin and commercial wound-healing hydrogels for in vivo wound-healing applications. (A) Wound closure rates of mice treated with distinct samples, including sundew-derived and -inspired adhesives and corresponding groups seeded with ADSCs, mucin, and cellulose. Positive control was selected from a commercial wound-healing hydrogel. The results show that the respective mice treated with sundew-derived or -inspired adhesive hydrogels exhibit similar wound-closure rates; the addition of ADSCs effects a significant improvement on accelerating the wound closure. Even compared to the positive group treated with a commercial wound-healing hydrogel, the ADSCs-added sundew-derived or -inspired adhesive hydrogels still possess a preferable wound-healing potential. (B) H&E stained sections of the wound skins treated with sundew-derived and -inspired adhesive hydrogels after 11 day tests. Samples treated with or without ADSC were evaluated, respectively. Further analysis demonstrates that the wounds treated with sundew-derived and -inspired adhesive hydrogels exhibit markedly higher rehabilitation rates as compared to those of untreated groups.

**Table 1**

Variable Concentrations of Sodium Alginate, Gum Arabic, and  $\text{Ca}^{2+}$  Were Used to Investigate the Bioinspired Adhesive Hydrogels<sup>a</sup>

names	sodium alginate (% w/v)	gum arabic (% w/v)	$\text{Ca}^{2+}$ (mM)
sodium alginate	4	0	0
gum arabic	0	4	0
S1G2	4/3	8/3	0
S2G1	8/3	4/3	0
S1G1	2	2	0
S1G1Ca5	2	2	5
S1G1Ca10	2	2	10
S1G1Ca15	2	2	15

<sup>a</sup>All of the samples have a 4% (w/v) total concentration.

Author Manuscript

Author Manuscript

Author Manuscript

Author Manuscript